Proceedings of the 20th National Conference on Superconductivity "New Phases, Concepts and Advances"

Ni-Driven Evolution of Pseudogap and Superconducting Gap in Underdoped Cuprate

A. Malinowski*, V.L. Bezusyy and P. Nowicki

Institute of Physics, Polish Academy of Sciences, al. Lotników 32/46, PL-02668 Warsaw, Poland

Doi: 10.12693/APhysPolA.143.134 *e-mail: artur.malinowski@ifpan.edu.pl

In the presented study, Ni impurity is used to probe pseudogap and superconducting gap in the underdoped cuprate $La_{1.85}Sr_{0.15}CuO_4$. The longitudinal magnetoresistance measurements reveal the presence of local maximum at the same temperature T_{max}, below which zero-field resistivity in the parallel-resistor model deviates from its T^2-dependence. Tracking the systematic evolution with Ni content y allows equating T_{max} with pseudogap temperature T^*. The rate of pseudogap closing by the magnetic field is consistent with the spin-paramagnetic effect, which is also the main pair-breaking process destroying superconductivity in the same field configuration. The thermal energy scale of pseudogap k_BT^* for $y = 0$ is equal to the relevant magnetic Zeeman energy scale. With increasing y, both energy scales separate from each other. The increased Stoner factor is partially responsible for the enhancement of the Pauli effect and the decrease of the Zeeman limiting field with increased y.

topics: cuprate superconductors, pseudogap, effects of doping, Pauli paramagnetic effect

1. Introduction

In underdoped cuprates, pseudogap energy scale k_BT^* grows with underdoping (decreasing carrier concentration p) while superconducting (sc) transition temperature T_c decreases. Since the early days of high-T_c, this dichotomy remains an obvious challenge for any theory attempting to find a possible relationship between the pseudogap (PG) and the superconducting gap (SCG) because, for the mean-field type phase transitions, the transition temperature is proportional to the corresponding energy scale of the given order parameter and lack of such relationship underscores the unconventional character of sc state in cuprates. After the subsequent discoveries of new sc compounds, it seems clear that any theory attempting to overarch three main unconventional sc families, i.e., heavy fermions, cuprates, and iron-based superconductors, must provide a transparent understanding of the pseudogap in cuprates [1]. Both the two distinctive gaps (antinodal PG and nodal SCG) scenarios [2, 3] and single d-wave energy gap models [4, 5] have been proposed. It is also possible that the antinodal and nodal gaps are correlated, with the former relevant to the formation of electron pairs and the latter related to their condensation, and with nodal-gap energy $2\Delta_N$ being proportional to the product of Δ^* and a square-root superfluid density [6]. A brief overview of the selected theories regarding the PG in cuprates can be found in [7].

This is a bit surprising after over 30 years since the first PG evidence from nuclear magnetic resonance [8, 9], but the question about the true location of the pseudogap line in the cuprate phase diagram still remains open [10]. The experimental data on $La_{2-x}Sr_xCuO_4$ (LSCO) published between 1990 and 2018 by thirteen distinct groups using a variety of experimental probes have been gathered in [11]. Even when the same technique is employed, the results can differ significantly. Although the up-to-date reports (based, among other things, on the resistivity measurements) estimate T^* in $La_{1.85}Sr_{0.15}CuO_4$ (LSCO15) as 130 ± 20 K ([12] and [13]), the analysis of temperature-derivative curves locates T^* for the same compound at ≈ 235 K (see [13] and [14]).

Some insights into the energy scales of both gaps in cuprates can be gained by probing the relevant magnetic scales. This, however, usually requires extremely large magnetic fields. The contactless conductivity measurements in the field up to 100 T applied parallel to the CuO_2 plane reveal that the Zeeman splitting energy of electron spin $2\mu_BB$ in optimally doped cuprate $La_{1.84}Sr_{0.16}CuO_4$ (LSCO16) becomes larger than SCG energy estimated from angle-resolved photoemission spectroscopy (ARPES) only above $B = 85$ T [15]. Clearly distinct but converted to the same pseudogap energy scale k_BT^*, the orbital and Zeeman limiting fields in $Bi_2Sr_2CaCu_2O_{8+\delta}$ (BSCCO), established from the measurements up to 60 T, favor

the picture where charge and spin degrees of freedom are separated onto different parts of the Fermi surface [16, 17].

The upper critical field in type-II superconductors can be predicted from the low-field dependence of T_c in the framework of Werthamer–Helfand–Hohenberg (WHH) theory [18, 19]. The model, originally derived from the adopted BCS model with a spherical Fermi surface, has been successfully applied recently to presumably *s*-wave iron-based superconductors [20, 21] and optimally doped *d*-wave cuprates [15, 22]. To what extent are the BSC-based models capable of grasping some aspects of underdoped cuprate physics remains an open question.

In this study, we compare the Ni-driven evolution of energy scales in LSCO15 characteristic for sc state with those relevant to PG, the manifestation of which in longitudinal magnetoresistance (LMR) we have found recently [23]. The Ni-induced enhancement of the PG energy scale accompanying suppression of superconductivity was observed in Ni-substituted underdoped $NdBa_2Cu_3O_{6.8}$ [24]. As noted, this is at variance not only with the theories seeing PG as a precursor sc phase but also with those that relate PG to charge or spin density waves [25, 26], because the latter models assume nesting of Fermi surface [27], which Ni should weaken. Ni impurity, when introduced into the LSCO conductive planes, exhibits a magnetic character starting from the smallest concentration y [28]. Thus, the rich magnetism of LSCNO has to be taken into account when the intrinsic properties of the CuO_2 planes are to be probed by Ni doping.

2. Experiment

The measurements were carried out on the thin $La_{1.85}Sr_{0.15}Cu_{1-y}Ni_yO_4$ (LSCNO) films deposited by laser ablation on $LaSrAlO_4$ substrates. The targets for ablation were prepared by a standard solid-state reaction method from the oxide powders of 4N–5N purity. The powders were preheated, mixed, and pressed into 10 g pellets, which were heated up to 1050°C and sintered at this temperature in flowing oxygen for 2 days. After regrounding the pellets, the whole procedure was repeated two more times. The X-ray powder diffraction analysis confirmed the tetragonal K_2NiF_4-type structure and revealed no impurity phases in the final targets [29, 30].

The LSCNO films with a thickness of about 1000 Å were grown with Nd:YAG laser. The deposition was carried out for 15 min in flowing oxygen under a pressure of 300 mTorr and at substrate temperature of 760°C. The standard Hall-bar structure was patterned by photolithography. More technological details are given elsewhere [23].

The magnetoresistance (MR) measurements were performed in a magnetic field up to 9 T in the commercial Quantum Design PPMS cryostat. Both the built-in PPMS electronics and 370 AC resistance bridge by Lake Shore connected through the patch box by Wimbush Science & Technology Ltd were used. Using the home-made 30 g cooper holder, which was placed on the top of the standard puck, turned out to be a key factor in improving temperature stabilization. The average of runs up and down in one field direction is used in the presented analysis. The resulting resistance fluctuations level is estimated to be below 10 ppm during 6 h of isotemperature field runs after 5 h of temperature stabilization. No correction was made for the original Quantum Design calibration of the main PPMS Cernox thermometer.

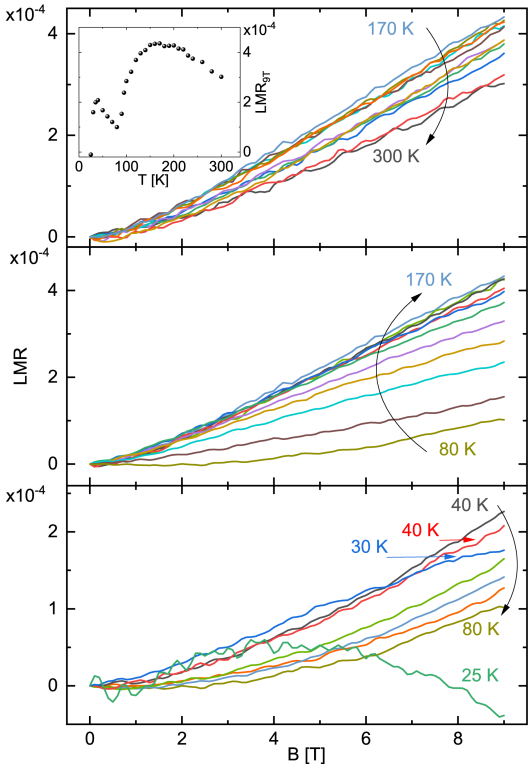

Fig. 1. Field dependence of LSCNO35 LMR. The inset shows LMR at 9 T as a function of temperature.

3. Results

The temperature dependence of LMR in the normal state of LSCNO exhibits a non-monotonic behavior in the whole investigated Ni content. An example of the LMR vs field curves at various temperatures is shown in Fig. 1 for the $y = 0.035$ sample (LSCNO35). As can be seen in the inset, positive LMR at $B = 9$ T increases with decreasing temperature down to the local maximum at around $T_{\max} = 170$ K, next starts to decrease, and after achieving a sharp minimum at around $T_{\min} = 80$ K, increases again. For larger y, a subsequent decrease of positive LMR at 9 T is a harbinger of negative LMR in the whole field range observed at the lowest T. For LSCNO35 and the samples with smaller Ni content, the further behavior of LMR

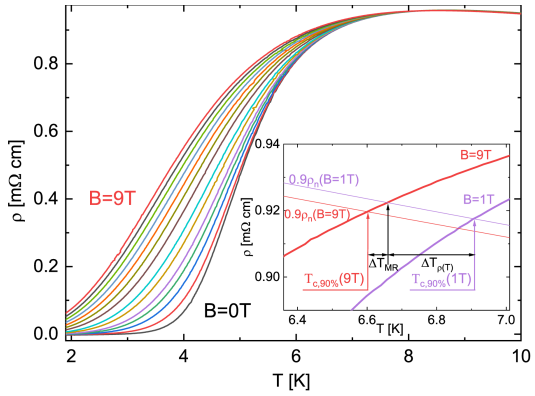

Fig. 2. Temperature dependence of LSCNO35 resistivity near sc transition at fields (bottom up) from 0 to 1 T every 0.25 T and 1.5 T and from 2 to 9 T every 1 T. The inset shows that difference between T_c at different fields can be formally regarded as a sum of $\Delta T_{\rho(T)}$ caused by temperature dependence of ρ_n and $\Delta T_{\rm MR}$ caused by negative MR above T_{crs}.

with decreasing T is affected by the presence of superconducting transition. For the nonsuperconducting samples, we observe a large negative LMR of the order of 10^{-2} at 2 K in the 9 T field, which can be related to the Kondo effect [31]. Temperature behavior of transverse MR mimics that of LMR suggesting that spin-related effects play the dominant role in both field configurations.

To elucidate Ni-influence on PG and SCG, we investigated superconducting transition in LSCNO35 in more detail. Such a level of doping substantially decreases T_c in the system and causes a field-induced change in T_c to be more pronounced in our B–T measurement window (Fig. 2). This, in its turn, facilitates making a prediction of orbital B_{c2} at $T = 0$ K utilizing the WHH model and estimation of Pauli paramagnetic effect [32, 33] through the Maki parameter α [34, 35].

Experimentally, α can be estimated from the slope $\mathrm{d}B_{c2}/\mathrm{d}T$ in the vicinity of T_c. Recalling the known problems with finding an exact value of *resistive* B_{c2} with sufficient accuracy, let us note that in both geometries of the experiment, the broadening of transition in LSCNO35 is quite substantial (Fig. 2). Thus, although the effect is the most distinct when the field is perpendicular to the CuO_2 plane (not shown), which can be easily reconciled with the presence of the vortex-liquid phase, using of the standard 90% ρ_n criterion (where ρ_n is normal-state resistivity just above the transition) is more reliable in constructing B_{c2} vs T diagram than any other criterion in *any* configuration.

The important issue that needs to be clarified is the influence of normal-state MR on B_{c2} estimation. In LSCNO35, the positive high-T LMR(9 T) becomes negative below 25 K (inset in Fig. 2). However, all the $\rho(T)$ curves at various fields intersect at $T_{crs} = 8.20 \pm 0.02$ K, and LMR becomes positive again below T_{crs}. The sheet resistance here, $R_{crs} = 0.088$ kΩ/□, is far below the quantum resistance $R = h/(2e)^2 = 6.45$ kΩ/□, and the crossing is simply a result of interplay between the sc fluctuations and the normal-state MR. Both ignoring MR (as in [36]) and taking MR into account (as in [37]) can strongly affect the observed deviations of B_{c2} vs T curves from the WHH theory [38].

In addition, LSCNO exhibits a pronounced dependence of ρ on T below its local minimum, even at zero field. To factor it in the analysis, we have interpolated normal-state $\rho(T)$ at all fields with a polynomial of 4th degree. The interpolated T-region spans from 50 down to 12.9 K, where $|\mathrm{d}\rho(T)/\mathrm{d}T|$ has its local maximum. Next, the so-obtained interpolating curves $\rho_n(T)$ have been extended down, outside the fitted T-region, and the chosen fraction of ρ_n has been tested as an sc-transition criterion. The two curves $0.9\rho_n(T)$ for $B = 1$ T and $B = 9$ T, depicted as the thin lines in the inset in Fig. 2, are given as an example to show that the proper extrapolation of $\rho_n(T)$ influences the reliable estimation of $T_c(B)$ much more than MR itself does, although both factors should be taken into account. At zero field, this procedure yields $T_c^{90\%} = 6.93 \pm 0.01$ K.

4. Discussion

4.1. Upper critical field in LSCNO35

The above detailed analysis allows us to construct a reliable B_{c2}–T diagram and compare it with the WHH theory predictions. According to the WHH model, the temperature dependence of the upper critical field $\mu_0 H_{c2}$ for an isotropic type-II superconductor in the dirty limit and in the general case including both orbital-limiting and Pauli-limiting effects can be obtained from the following equation [35]

$$\ln\left(\frac{1}{t}\right) = \left(\frac{1}{2}+\frac{\mathrm{i}\lambda_{\rm so}}{4\gamma}\right)\psi\left(\frac{1}{2}+\frac{\overline{h}+\lambda_{\rm so}/2+\mathrm{i}\gamma}{2t}\right) + \left(\frac{1}{2}-\frac{\mathrm{i}\lambda_{\rm so}}{4\gamma}\right)\psi\left(\frac{1}{2}+\frac{\overline{h}+\lambda_{\rm so}/2-\mathrm{i}\gamma}{2t}\right) - \psi\left(\frac{1}{2}\right). \tag{1}$$

Here, the Maki parameter α describes the relative influence of the orbital- and Pauli-limiting effects, the spin–orbit scattering strength is given by the parameter $\lambda_{\rm so}$, and magnetic field $\mu_0 H_{c2}$ is introduced as the reduced parameter

$$\overline{h} = \frac{4}{\pi^2}\frac{H_{c2}}{T_c\left(-\frac{\mathrm{d}H_{c2}}{\mathrm{d}T}\right)\Big|_{T_c}} \tag{2}$$

into the arguments of digamma function and into the term $\gamma = [(\alpha\overline{h})^2-(\lambda_{\rm so})^2]^{1/2}$. Following the standard practice [15, 39], we adjusted the parameters α and λ_s to get the best fit of (1) to the experimental data.

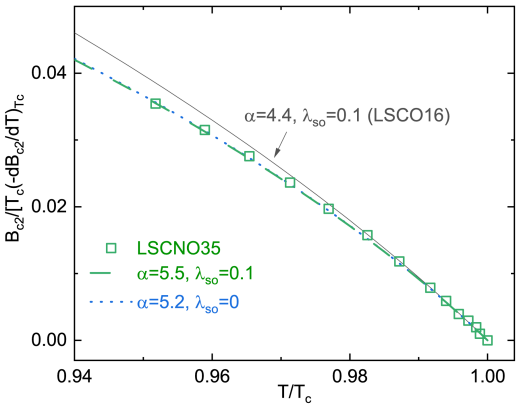

Fig. 3. Normalized upper critical field of LSCNO35 as a function of reduced temperature. The lines depict the solutions of (1) for the indicated parameters.

The orbital limited upper critical field B_{c2}^{orb} in the $T = 0$ K limit can be calculated from the slope of this curve at T_c

$$B_{c2}^{orb}(0) = -0.693 \left(\frac{\mathrm{d}B_{c2}}{\mathrm{d}T} \right) \Big|_{T_c} T_c. \qquad (3)$$

The calculated $\mathrm{d}B_{c2}/\mathrm{d}T = -36.6$ T/K yields $B_{c2}^{orb} = 176$ T, which is much above $B_{c2} = 85$ T (at $T = 4.2$ K) directly measured in LSCO16 [15]. Even in our very limited t range, the experimental data at the larger field (smaller t) are clearly below the WHH curve for the parameters found for LSCO16 in [15], $\alpha = 4.4$ and $\lambda_{\mathrm{so}} = 0.1$. Employing larger $\alpha = 5.5$ and the same $\lambda_{\mathrm{so}} = 0.1$ gives a better description of the data, and this set of parameters is the final WHH prediction for $B_{c2}^{orb}(t)$ in LSCNO35. Simultaneously, zero-temperature Pauli limited field $B^{\mathrm{Pauli}}(0)$ can be calculated as $B^{\mathrm{Pauli}}(0) = \sqrt{2}B_{c2}^{orb}(0)/\alpha \simeq 45$ T [34].

Actually, $\lambda_{\mathrm{so}} = 0.1$ for LSCO16 is the *upper limit* of λ_{so} estimated from the large-field measurements [15]. It is known that α and λ_{so} affect the shape of the WHH curve in a similar fashion [40]. The changes, although not identical, work against each other, which makes it difficult to differentiate the origins of the effects [41]. While increasing α increases the flattening of the $B_{c2}(t)$ curve at low t, the spin-orbit scattering can partially reduce this effect. The dotted line in Fig. 3 is the WHH curve calculated for $\alpha = 5.2$ and $\lambda_{\mathrm{so}} = 0$. This line is hardly distinguished from the previous curve and thus gives a natural estimation of the uncertainties in the obtained results.

For sure, the known effect of α increase for disordered systems contributes to larger α for LSNO35 when compared with LSCO16 in the same field geometry. Since α in the WHH theory depends on the Fermi velocity v_{F} and the scattering time τ as $\alpha = 3\hbar/(2m_e v_{\mathrm{F}}^2 \tau)$, the straightforward explanation for enhanced α is decreasing of mean free path $v_{\mathrm{F}}\tau$ caused by the Ni ions being the strong scattering centers.

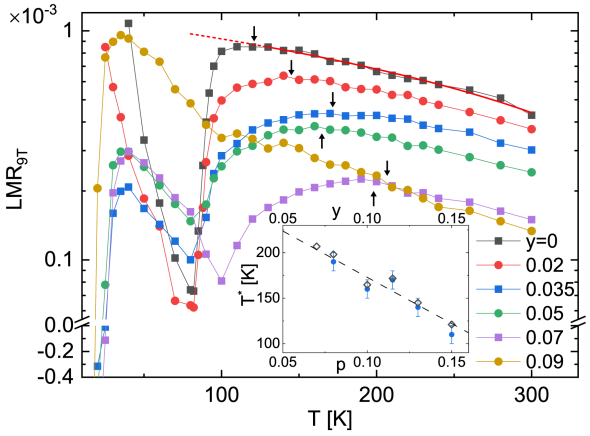

Fig. 4. Temperature dependence of LMR at $B = 9$ T in LSCNO with various Ni content y. The red solid line is a best fit of exponential function to LSCO15 data above the transition, extended down to 80 K (the dashed part of the line). The inset shows the pseudogap temperature T^* as a function of mobile carrier concentration p (bottom scale) or Ni concentration y (upper scale). The black open diamonds mark T_{dev} indicated by the black arrows in the main panel, the blue circles — the temperature of local LMR maximum, and the dashed line — $T^*(p)$ from [12].

Despite the limited capabilities of the WHH model for a proper description of $B_{c2}(t)$ in d-wave cuprates, it has been possible to reconcile the experimental results in LSCO16 with the WHH predictions from the low-field data using the scaling factor $s = 1.5$ [15]. Following the argumentation and employing the same s, we estimated $B_{c2}(0)$ in LSCNO35 as $\simeq 56$ T in the discussed longitudinal configuration.

4.2. Determination of pseudogap opening temperature

Now we can revert to pseudogap to compare its field dependence with the estimated B_{c2}.

LMR in the T-region above the temperature of local maximum $T_{\max}$ increases exponentially with decreased temperature. This is depicted in Fig. 4 for the 9 T field but remains true for the lower fields as well. The linear fits on the log scale can be extended down and utilized to estimate the relative change in LMR at the transition in a given field. Therefore,

$$\delta\mathrm{LMR} = \frac{\mathrm{LMR}_{ext} - \mathrm{LMR}_{\min}}{\mathrm{LMR}_{ext}}, \qquad (4)$$

and $T_{\min}$ is here the temperature of the local minimum in the LMR vs T curve (equal to ≈ 80 K for $y = 0$ and ≈ 100 K for $y = 0.07$), and LMR_{ext} is the predicted value of LMR that would be at $T_{\min}$ if the PG had not opened below $T_{\max}$. In the following, we will show that $T_{\max}$ can be equated with the pseudogap opening temperature T^*.

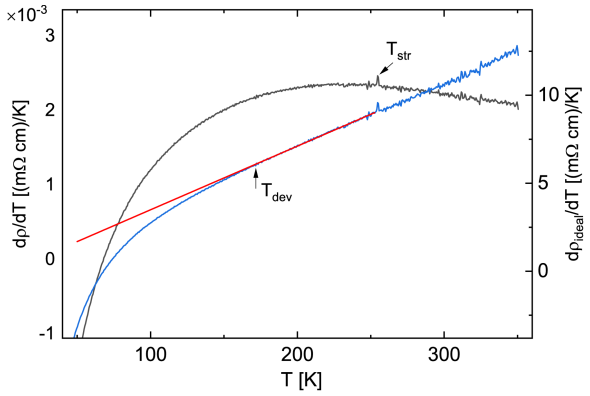

Fig. 5. The derivatives of the raw resistivity data and the ideal resistivity in the absence of saturation for LSCNO35.

In the whole Ni-content range studied here, δLMR decreases linearly with the increased field. The reduction of LMR anomaly becomes larger for larger y and comes to about 0.7 at $B = 9$ T for $y = 0.07$. This means that estimation of the field B_{pc} at which $\delta\mathrm{LMR} = 0$, which can be regarded as an indication of pseudogap closing, requires linear extrapolation far above the field accessible in the experiment. Such a procedure yields $B_{pc} \simeq 79$ T for $y = 0$ and $B_{pc} \simeq 50$ T for $y = 0.035$. Both values are close to the predictions of the upper critical field for the superconducting gap in these compounds. Namely, B_{c2} measured on LSCO16 crystal with $T_c = 36.7$ K is equal to 85 T (at 4.2 K), and one can expect a similar value for LSCO15 film with similar $T_c^{90\%} = 36.3$ K. For $y = 0.035$, as mentioned above, $B_{c2} \cong 56$ T.

There is no obvious feature in zero-field resistivity that could be directly linked to such a prominent maximum in LMR. Even the derivatives of raw data, $\mathrm{d}\rho/\mathrm{d}T$, seem to be smooth and featureless in the region near $T_{\max}$. It is illustrated for LSCNO35 in Fig. 5. The peak at $T_{str} = 255$ K, which is much higher than $T_{\max}$, indicates the structural transition and will be addressed further. However, we have shown very recently that taking Ioffe–Regel–Mott (IRM) limit into account reveals the existence of a weak yet visible feature in zero-field transport, which temperature T_{dev} correlates very well with $T_{\max}$ [23].

Although the existence of the IRM limit in cuprates remains a subject of debate [42], the parallel resistor formula, stemming from the minimal scattering time being an equivalent of the minimal conductivity $1/\rho_{\mathrm{IRM}}$, is a very accurate description of $\rho(T)$ dependence in LSCNO above ~ 150 K [29]

$$\frac{1}{\rho(T)} = \frac{1}{\rho_{\mathrm{ideal}}} + \frac{1}{\rho_{sat}} \equiv \frac{1}{a_0 + a_1 T + a_2 T^2} + \frac{1}{\rho_{sat}}. \tag{5}$$

Decreasing of $\mathrm{d}\rho/\mathrm{d}T$ with increasing temperature, visible for LSCO35 already above ≈ 240 K (Fig. 5), is a sign of resistivity saturation at ρ_{sat}. The fitted ρ_{sat} agrees well with ρ_{IRM} calculated within the Boltzmann theory for the so-called "small" Fermi surface with n holes (in opposition to the "large" one with $n + 1$ holes). Our thermopower measurements reveal that the concentration of mobile holes n decreases with increased y and $n = 0.15 - y$. This is caused by immobilizing the hole by Ni ion, resulting in the localized Zhang–Rice doublet state [43], as shown in the X-ray-absorption fine structure measurements of local distortions around Ni in LSCNO single crystals [44].

Both the fitted ρ_{sat} and the calculated ρ_{IRM} can be utilized to find the temperature T_{dev}, where $\mathrm{d}\rho_{\mathrm{ideal}}/\mathrm{d}T$ deviates downward from the high-T T^2-dependence. Both ways give consistent results, but using ρ_{sat} eliminates the errors caused by the uncertainties in the geometric factor for resistivity. After subtracting $1/\rho_{sat}$ from the raw conductivity data, the derivative is calculated and fitted repeatedly by the straight line below T_{str} down to the subsequent T-points. When all the data points are below the low-T extension of the fitted line, this T-point is taken as T_{dev}. This simple yet very precise procedure allows establishing T_{dev} with the precision of the order of 1 K.

The striking coincidence between $T_{\max}$ from the LMR measurements and T_{dev} from zero-field transport is depicted in the inset in Fig. 4. As can be seen, the n-dependence of $T_{dev} \simeq T_{\max}$ closely follows the T^* vs p line from Fig. 1 in [12] when one equates n with hole concentration p from the cuprate phase diagram. This justifies equating these two characteristic temperatures with the PG opening temperature T^*.

The sharp peak mentioned above, visible in the derivatives at $T_{str} = 255$ K, indicates the structural transition from the high-temperature tetragonal phase to the low-T phase with the lower symmetry. Since the p-dependence of T_{str} in LSCO crystals is similar to that for T^*, this may lead to misinterpretation of the resistivity second-derivatives maps used in the literature to find the precise location of T^*. In the LSCNO films, presumably, clamping the films by substrate makes the external dimensions of the unit cell intact, and the structural transition at T_{str} involves only the changes in the internal symmetry of the cell. No systematic change of T_{str} with y was observed in the LSCNO films. Our X-ray measurements at room temperature reveal that the c-axis lattice constant decreases with increased y and the rates $\mathrm{d}c/\mathrm{d}y$ for the films are similar to those for the targets (the difference is below 8%). Thus the compressive in-plane strain resulting from the stress caused by the smaller lattice constant of the substrate does not change much with y, and the sample-depended variations can be comparable to this systematic change. The above seems to be a reasonable explanation for the lack of systematic change in T_{str} with y. More details can be found in Appendix D in [23].

4.3. Enhancement of spin-paramagnetic effect

In Fig. 6, we compare the characteristic temperature and energy scales for both gaps in LSCNO. While T^* and T_c clearly exhibit the opposite trends with y, the magnetic scales corresponding to PG and SCG coincide for $y = 0$, and both decrease in the same manner with increased y. The measured T_c is transformed into the SCG magnitude through the d-wave BCS relationship $E_{\rm sc} = 2\Delta_{\rm sc} = 4.3k_{\rm B}T_c$ [3]. So calculated $\Delta_{\rm sc}(y = 0)$ yields Chandrasekhar–Clogston limit $B^{\rm Pauli}(0\ {\rm K}) = 79$ T, which is close to $B_{c2} = 85$ T directly measured in LSCO16 and results in similar equivalent Zeeman energy $g\mu_{\rm B}B_{c2}$ (open circle and diamond in Fig. 6, respectively).

For pseudogap, the same BCS-like relationship $2\Delta^* = 4.3k_{\rm B}T^*$ was found to be approximately fulfilled in LSCO and $Bi_2Sr_2CuO_{6+\delta}$ (Bi2201), and as a result Δ^*, was suggested to be universal for single-layer cuprates [3]. The characteristic magnetic scale is given by B_{pc}, and the corresponding Zeeman energy for LSCO15 matches that established by T^* when the simple scaling relationship $g\mu_{\rm B}B_{pc} = k_{\rm B}T^*$ ($g = 2$) is employed. The measurements of B_{pc} on the other single-layer cuprates are needed to verify the hypothesis about the universality of Δ^* and the possible interconnection of the relevant energy scales.

Replacing 3.5% of Cu ions with Ni reduces $B^{\rm Pauli}(0)$ from 68 down to 45 T, while in a dirty BCS superconductor, $B^{\rm Pauli}(0)$ is independent of the impurities [45]. Looking for the origin of enhancement of the Pauli paramagnetic effect, it is instructive to consider the possible change in the Stoner enhancement factor $S = \chi_s/\chi_{\rm P}$. Due to strong electron–electron interactions, the magnetic susceptibility of the carrier spins in the system, χ_s, can deviate from the simple Pauli paramagnetism formula $\chi_{\rm P} = \mu_{\rm B}^2\, N(E_{\rm F})$ and become T-dependent.

Magnetic susceptibility χ of the polycrystalline LSCNO samples (cut from the targets used for the fabrication of the thin films) may be decomposed into three terms [28, 46]

$$\chi = \chi_0 + \chi_{\rm spin}(T) + \frac{C}{T}, \qquad (6)$$

where χ_0 is the T-independent part, $\chi_{\rm spin}(T)$ comes from the 1/2 spin antiferromagnetic (AF) lattice formed in the CuO_2 plane and can be described by the universal empirical curve, and the Curie term reflects the additional magnetic moment introduced by Ni ions [47, 48]. Although such an *independent moment scenario* may be questionable, the fits of this model to $\chi(T)$ curves for Zn-doped are hardly distinguished from those in *quasi-particle resonance scenario* [49]. The temperature independent χ_0 consists of three terms: diamagnetic susceptibility of the core $\chi^{\rm core}$, orbital Van Vleck susceptibility $\chi^{\rm VV}$,

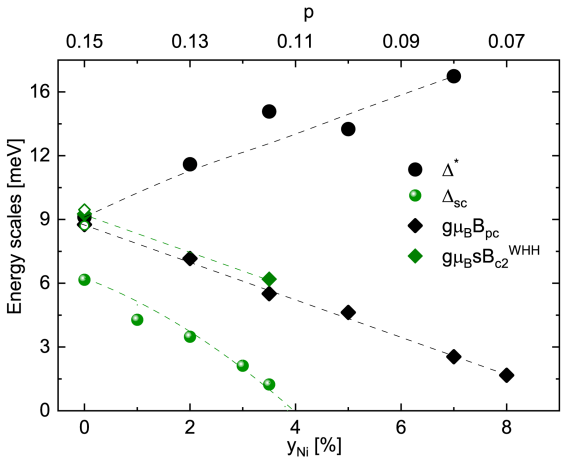

Fig. 6. Ni-doping dependence of the characteristic energies in LSCNO. Green (black) symbols denote superconducting (pseudogap) parameters. The dashed lines are guides for the eye; open symbols — see text.

and the Pauli susceptibility contribution from the doped carrier spins $\chi^{\rm Pauli}$ (together with the possible Landau diamagnetism contribution). The analysis of ^{63}Cu NMR Knight shifts demonstrates that local Cu^{2+} moments in LSCO are strongly coupled to the carrier spins [50]. If so, re-grouping the terms in (6) as

$$\chi(T) - \frac{C}{T} = \chi^{\rm core} + \chi^{\rm VV} + \chi_s(T), \qquad (7)$$

where $\chi_s(T)$ stands for spin susceptibility, shows more clearly the spin-orbit partition of LSCNO susceptibility [51]. The Curie-like term needs to be subtracted to obtain the intrinsic spin susceptibility of hole-doped CuO_2 planes. The measured $\chi(T)$ in LSCO15 does not change very much between 300 and 400 K ($\approx 1\%$) and increases with y from $\chi(y{=}0) = 1.08 \times 10^{-4}$ emu/(Oe mole) to $\chi(y{=}0.035) = 1.46 \times 10^{-4}$ emu/(Oe mole). As $\chi^{\rm VV}(y{=}0)$ we took χ for Sc_2CuO_4, 2.3×10^{-5} emu/(Oe mole) [52]. Taking $\chi_{\rm P} \approx 0.7 \times 10^{-4}$ emu/(Oe mole) from the band theoretical calculations [51, 53] for LSCO15 yields $S \approx 2.6$, which is larger than $S = 2.0$–2.3 (at 320 K) reported for LSCO with $x = 0.13$–0.18 in [51]. Substitution of y Ni^{2+} ions having $3d^8$ shell ($\chi^{\rm VV} \approx 5{\times}10^{-5}$ emu/(Oe mole) [54] with Cu^{2+} ions having still incomplete $3d^9$ shell increases $\chi^{\rm VV}$ of the system as $\chi^{\rm VV}$ [10^{-5} emu/(Oe mole)] $= 2.3(1{-}y) + 5y$. For $y{=}0.035$ this gives $\chi^{\rm VV} = 2.4 \times 10^{-5}$ emu/(Oe mole). The diamagnetic inner-shell electron contribution $\chi^{\rm core} = -9.8 \times 10^{-5}$ emu/(Oe mole) [51] is not altered. Finally, this leads to the linear increase of the spin susceptibility

[†1] Calculated for $T_c^{50\%} = 34.6$ K. For $T_c^{90\%} = 36.3$ K, $B^{\rm Pauli}(0\ {\rm K}) = 82$ T.

[†2] χ for $y = 0.035$ is interpolation of the results for targets from [28].

χ_s from 1.8×10^{-4} emu/(Oe mole) with the average rate $(1.1\pm0.3)\times10^{-5}$ emu/(Oe mole) per 1% of Ni when y is increased from 0 up to 0.07, and the measured $\chi(y)$ at 300 K [28] is used. So calculated ratio $\chi_s(y{=}0.035)/\chi_s(y=0)$ is equal to $\simeq 1.2$ at 300 K.

Remaining still in the framework of the BCS model, $B^{\rm Pauli}(0)$ in such a system with strong electron–boson and electron–electron interactions is given by [21, 45, 55]

$$B^{\rm Pauli}(0) = \frac{1.86T_c}{S}\left(1+\lambda\right)^{\varepsilon}\eta_\Delta\,\eta_{ib}, \qquad (8)$$

where η_Δ is the strong intraband correction for the isotropic s-wave gap Δ, anisotropy effects of which are described by η_{ib} that phenomenologically includes also the additional factors as energy dependence of states, etc., λ is electron–boson coupling constant, and $\varepsilon = 0.5$ or 1. Only on the assumption that the numerator in (8) does not vary, the *whole* change in $B^{\rm Pauli}(0)$ can be ascribed to a change in S. While the parent expression, i.e., Chandrasekhar–Clogston limit $B^{\rm Pauli}(0) = \Delta/(\sqrt{g}\mu_{\rm B})$ shows more directly that $B^{\rm Pauli}(0)$ follows Δ dependence in BCS theory, the derivative of (8) demonstrates that increased S acts on $B^{\rm Pauli}$ in the same direction as decreased Δ.

Looking at the formula for S from the random phase approximation for the effective interaction I (i.e., $S = 1/[1{-}I\,N(E_{\rm F})]$, where $N(E_{\rm F})$ is the density of states at the Fermi level), one can see that S can increase via an increase of I or $N(E_F)$. Given the lack of ARPES data for LSCNO, we can only state that our thermopower measurements do not give any indications of the change of $N(E_F)$ with Ni doping [29]. Thus the reason for the $B^{\rm Pauli}$ decrease seems to lie in the enhancement of the effective exchange integral I. Trapping the mobile holes by Ni ions can locally restore the AF correlations leading to an increase in the effective I [28].

On the basis of a crude comparison between parent compounds of cuprates and nickelates, La_2CuO_4 (LCO) and La_2NiO_4 (LNO), one can say that the trend seen in $S(y)$ is in accordance with the change in charge transfer gap Δ_{ct} between LCO and LNO. In the 2D t–J model [56], χ_s is expressed as $\chi_s = \chi_{\rm P}/[1 + J\,N(E_{\rm F})]$, and a superexchange interaction J plays a role of the effective interaction I in the Stoner factor [57]. The superexchange interaction J of a charge transfer type in the transition-metal compounds depends on Δ_{ct} and Coulomb interaction U as [58]

$$J \propto \frac{1}{\Delta_{ct}^2}\left(\frac{1}{\Delta_{ct}} + \frac{1}{U}\right). \qquad (9)$$

Since $\Delta_{ct} \approx 4$ eV in LNO is about twice that of LCO [59, 60], J is expected to decrease and thus χ_s to increase when passing from cuprate to nickelate. This agrees with the trend observed in LSCNO with increasing y.

The y-dependencies of the characteristic energy scales in LSCNO depicted in Fig. 6 seem to be reminiscent of p-dependencies in the LSCO phase diagram. In particular, B_{c2} decreases with increased y (decreased p). Competing orders were suggested as a reason for non-monotonic but overall decreasing tendency with decreasing p in Eu-LSCO and YBCO since B_{c2} has its local minimum at $p = 0.11$, where stripe order is strong. While effective doping level $p = 0.15{-}y$ is certainly the leading factor in the evolution of the energy scales in LSCNO, it seems highly improbable that effective underdoping caused by adding Ni ions reconstructs all details of generic cuprate diagram, together with all orders present on the underdoped side. Rather, this is an increased Stoner factor that plays a role in the enhancement of $B^{\rm Pauli}$ with increased y in LSCNO. This tendency is in contradiction with that found in LSCO, where decreasing of B_{c2} with underdoping is accompanied by a decrease in χ_s, and thus a decrease in S factor as well [47, 51].

5. Conclusions

In summary, the magnetotransport study on Ni-doped LSCO15 allowed us to find a manifestation of pseudogap opening in longitudinal magnetoresistance of the underdoped cuprate. The temperature of the local maximum in LMR correlates very well with the temperature of zero-field anomaly, which becomes apparent when the IRM limit in resistivity is taken into account. The similar sensitivity of PG and SCG to magnetic field parallel to the CuO_2 plane, anticipated from the low-field prediction of B_{c2} and B_{pc}, and the Zeeman relationship between T^* and B_{pc} in LSCO15 corroborate the presence of the spin-singlet correlations in the pseudogap phase. Although this is the mobile carrier concentration, decreasing with increasing Ni content, which governs the phase diagram of LSCNO, the increased Stoner factor seems to be partially responsible for the separation of pseudogap energy scale $k_{\rm B}T^*$ from the equivalent Zeeman energies $2\mu_{\rm B}B_{pc}$ and $2\mu_B B_{c2}$ of both gaps, too.

References

[1] N. Singh, *Physica C* **580**, 1353782 (2021).

[2] G. Deutscher, *Nature* **397**, 410 (1999).

[3] T. Yoshida, M. Hashimoto, S. Ideta et al., *Phys. Rev. Lett.* **103**, 037004 (2009).

[4] A. Kanigel, M.R. Norman, M. Randeria et al., *Nat. Phys.* **2**, 447 (2006).

[5] M.R. Norman, A. Kanigel, M. Randeria, U. Chatterjee, J.C. Campuzano, *Phys. Rev. B* **76**, 174501 (2007).

[6] H. Anzai, A. Ino, M. Arita, H. Namatame, M. Taniguchi, M. Ishikado, K. Fujita, S. Ishida, S. Uchida, *Nat. Commun.* **4**, 1815 (2013).

[7] A.A. Kordyuk, *Low Temp. Phys.* **41**, 319 (2015).

[8] W.W. Warren, R.E. Walstedt, G.F. Brennert, R.J. Cava, R. Tycko, R.F. Bell, G. Dabbagh, *Phys. Rev. Lett.* **62**, 1193 (1989).

[9] H. Alloul, T. Ohno, P. Mendels, *Phys. Rev. Lett.* **63**, 1700 (1989).

[10] Y. Noat, A. Mauger, M. Nohara, H. Eisaki, S. Ishida, W. Sacks, *Solid State Commun.* **348–349**, 114689 (2022).

[11] V. Sacksteder, *J. Supercond. Novel Magn.* **33**, 43 (2020).

[12] N. Doiron-Leyraud, O. Cyr-Choini'ere, S. Badoux et al., *Nat. Commun.* **8**, 2044 (2017).

[13] N.E. Hussey, R.A. Cooper, X. Xu, Y. Wang, I. Mouzopoulou, B. Vignolle, C. Proust, *Philos. Trans. Royal Soc. A* **369**, 1626 (2011).

[14] Y. Ando, S. Komiya, K. Segawa, S. Ono, Y. Kurita, *Phys. Rev. Lett.* **93**, 267001 (2004).

[15] D. Nakamura, T. Adachi, K. Omori, Y. Koike, S. Takeyama, *Sci. Rep.* **9**, 16949 (2019).

[16] T. Shibauchi, L. Krusin-Elbaum, M. Li, M.P. Maley, P.H. Kes, *Phys. Rev. Lett.* **86**, 5763 (2001).

[17] L. Krusin-Elbaum, T. Shibauchi, C.H. Mielke, *Phys. Rev. Lett.* **92**, 097005 (2004).

[18] E. Helfand, N.R. Werthamer, *Phys. Rev. Lett.* **13**, 686 (1964).

[19] E. Helfand, N.R. Werthamer, *Phys. Rev.* **147**, 288 (1966).

[20] H. Lei, R. Hu, E.S. Choi, J.B. Warren, C. Petrovic, *Phys. Rev. B* **81**, 094518 (2010).

[21] G. Fuchs, S.-L. Drechsler, N. Kozlova et al., *Phys. Rev. Lett.* **101**, 237003 (2008).

[22] T. Sekitani, Y.H. Matsuda, N. Miura, *New J. Phys.* **9**, 010047 (2007).

[23] A. Malinowski, V.L. Bezusyy, P. Nowicki, *J. Phys. Condens. Matter* **34**, 415602 (2022).

[24] A.V. Pimenov, A.V. Boris, L. Yu, V. Hinkov, T. Wolf, J.L. Tallon, B. Keimer, C. Bernhard, *Phys. Rev. Lett.* **94**, 227003 (2005).

[25] A.V. Chubukov J. Schmalian, *Phys. Rev. B* **57**, R11085 (1998).

[26] I. Affleck and J. B. Marston, *Phys. Rev. B* **37**, 3774 (1988).

[27] A. Gabovich, A. Voitenko, T. Ekino, M.S. Li, H. Szymczak, M. Pkaa, *Adv. Condens. Matter Phys.* **2010**, 681070 (2010).

[28] A. Malinowski, V.L. Bezusyy, R. Minikayev, P. Dziawa, Y. Syryanyy, M. Sawicki, *Phys. Rev. B* **84**, 024409 (2011).

[29] A. Malinowski, V.L. Bezusyy, P. Nowicki, *Phys. Rev. B* **95**, 014521 (2017).

[30] R. Minikayev, V. Bezusyy, A. Malinowski, *X-Ray Spectrom.* **44**, 389 (2015).

[31] K. Suzuki, T. Adachi, Y. Tanabe, Y. Koike, T. Kawamata, Risdiana, T. Suzuki, I. Watanabe, *Phys. Rev. B* **82**, 054519 (2010).

[32] A.M. Clogston, *Phys. Rev. Lett.* **9**, 266 (1962).

[33] B.S. Chandrasekhar, *Appl. Phys. Lett.* **1**, 7 (1962).

[34] K. Maki, *Phys. Rev.* **148**, 362 (1966).

[35] N.R. Werthamer, E. Helfand, P.C. Hohenberg, *Phys. Rev.* **147**, 295 (1966).

[36] F. Hunte, J. Jaroszynski, A. Gurevich, D.C. Larbalestier, R. Jin, A.S. Sefat, M.A. McGuire, B.C. Sales, D.K. Christen, D. Mandrus, *Nature* **453**, 903 (2008).

[37] S.I. Vedeneev, A.G.M. Jansen, E. Haanappel, P. Wyder, *Phys. Rev. B* **60**, 12467 (1999).

[38] G. Fuchs, S.-L. Drechsler, N. Kozlova, M. Bartkowiak, J.E. Hamann-Borrero, G. Behr, K. Nenkov, H.-H. Klauss, H. Maeter, A. Amato, *New J. Phys.* **11**, 075007 (2009).

[39] J.-l. Zhang, L. Jiao, Y. Chen, H.-Q. Yuan, *Front. Phys.* **6**, 463 (2011).

[40] M. Nikolo, J. Singleton, D. Solenov, J. Jiang, J.D. Weiss, E.E. Hellstrom, *J. Supercond. Novel Magn.* **30**, 331 (2017).

[41] D. Solenov, M. Nikolo, J. Singleton, J. Jiang, J. Weiss, E. Hellstrom, *AIP Conf. Proc.* **1895**, 060004 (2017).

[42] O. Gunnarsson, M. Calandra, J.E. Han, *Rev. Mod. Phys.* **75**, 1085 (2003).

[43] F.C. Zhang, T.M. Rice, *Phys. Rev. B* **37**, 3759 (1988).

[44] H. Hiraka, D. Matsumura, Y. Nishihata, J. Mizuki, K. Yamada, *Phys. Rev. Lett.* **102**, 037002 (2009).

[45] M. Schossmann, J.P. Carbotte, *Phys. Rev. B* **39**, 4210 (1989).

[46] V.L. Bezusyy, A. Malinowski, R. Minikayev, W. Paszkowicz, P. Dziawa, R. Gorzelniak, *Acta Phys. Pol. A* **118**, 402 (2010).

[47] D.C. Johnston, *Phys. Rev. Lett.* **62**, 957 (1989).

[48] T. Nakano, N. Momono, T. Nagata, M. Oda, M. Ido, *Phys. Rev. B* **58**, 5831 (1998).

[49] R. Islam, S. Naqib, *Physica C* **470**, 79 (2010).

[50] Y.-Q. Song, M.A. Kennard, K.R. Poeppelmeier, W.P. Halperin, *Phys. Rev. Lett.* **70**, 3131 (1993).

[51] Y. Itoh, T. Machi, A. Yamamoto, *Phys. Rev. B* **96**, 235118 (2017).

[52] T.C. Leung, X.W. Wang, B.N. Harmon, *Phys. Rev. B* **37**, 384 (1988).

[53] P.B. Allen, W.E. Pickett, H. Krakauer, *Phys. Rev. B* **36**, 3926 (1987).

[54] R. Klingeler, B. Büchner, S.-W. Cheong, M. Hücker, *Phys. Rev. B* **72**, 104424 (2005).

[55] T.P. Orlando, E.J. McNiff, S. Foner, M.R. Beasley, *Phys. Rev. B* **19**, 4545 (1979).

[56] J. Spalek, *Acta Phys. Pol. A* **111**, 409 (2007).

[57] T. Tanamoto, H. Kohno, H. Fukuyama, *J. Phys. Soc. Jpn.* **62**, 717 (1993).

[58] J. Zaanen, G. Sawatzky, *Can. J. Phys.* **65**, 1262 (1987).

[59] J.M. Tranquada, Y. Kong, J.E. Lorenzo, D.J. Buttrey, D.E. Rice, V. Sachan, *Phys. Rev. B* **50**, 6340 (1994).

[60] J.M. Tranquada, *AIP Conf. Proc.* **1550**, 114 (2013).